



Evidence of isospin-symmetry violation in high-energy collisions of atomic nuclei

The NA61/SHINE Collaboration

Strong interactions preserve an approximate isospin symmetry between up (u) and down (d) quarks, part of the more general flavor symmetry. In the case of K meson production, if this isospin symmetry were exact, it would result in equal numbers of charged (K^+ and K^-) and neutral (K^0 and \bar{K}^0) mesons in the final state. Here, we report results on the relative abundance of charged over neutral K meson production in argon and scandium nuclei collisions at a center-of-mass energy of 11.9 GeV per nucleon pair. We find that the production of K^+ and K^- mesons at mid-rapidity is $(18.4 \pm 6.1)\%$ higher than that of the neutral K mesons. Although with large uncertainties, earlier data on nucleus-nucleus collisions in the collision center-of-mass energy range $2.6 < \sqrt{s_{NN}} < 200$ GeV are consistent with the present result. Using well-established models for hadron production, we demonstrate that known isospin-symmetry breaking effects and the initial nuclei containing more neutrons than protons lead only to a small (few percent) deviation of the charged-to-neutral kaon ratio from unity at high energies. Thus, they cannot explain the measurements. The significance of the flavor-symmetry violation beyond the known effects is 4.7σ when the compilation of world data with uncertainties quoted by the experiments is used. New systematic, high-precision measurements and theoretical efforts are needed to establish the origin of the observed large isospin-symmetry breaking.

Keywords: quarks, strong interaction, isospin symmetry, flavor symmetry, nucleus-nucleus collisions, strange meson production

1 Introduction

One of the main aims of basic research is to understand the fundamental constituents of matter and the interactions between them. Within Quantum Chromodynamics (QCD) [1], the theory of strong interactions, the fundamental particles are quarks and gluons carrying color – the charge of strong interactions. Because of confinement, quarks and gluons are hidden in colorless hadrons, particularly protons and neutrons. The strong force binds them, forming atomic nuclei.

Accelerator-based experiments recording collisions of highly energetic hadrons and nuclei allow for systematic studies of the properties of strong interactions. In these collisions, many new particles are produced. They are predominantly mesons containing one valence quark (q) and one valence anti-quark (\bar{q}). The most copiously produced are the lightest mesons, pions and kaons, build from up (u), down (d) and strange (s) quarks and the corresponding anti-quarks.

QCD assumes that interactions are independent of quark type (flavor) in the limit of massless quarks and the absence of other interactions, a feature known as flavor symmetry. When only the light quarks up and down are considered, flavor symmetry reduces to isospin symmetry, historically introduced in the pre-QCD period by Heisenberg to understand the properties of nuclei [2]. The masses of up and down quarks¹, $m_u = 2.16 \pm 0.07$ MeV and $m_d = 4.70 \pm 0.07$ MeV [3], are neither vanishing nor equal, but they are much smaller than the QCD scale, Λ_{QCD} [4, 5]. Hence isospin-symmetry breaking effects are small, as confirmed by the mass ratios of pions and kaons, $(m_{\pi^+} - m_{\pi^0}) / (m_{\pi^+} + m_{\pi^0}) \simeq 0.017$ and $(m_{K^+} - m_{K^0}) / (m_{K^+} + m_{K^0}) \simeq -0.004$. Moreover, the elastic cross sections for pion-pion, pion-nucleon, and nucleon-nucleon scattering closely follow the predictions of isospin symmetry [6, 7]. Here, of special interest is a specific isospin transformation, an inversion of the third component of the isospin, called the "charge transformation" for historical reasons. It is equivalent to swapping $u \leftrightarrow d$ quarks. At the hadronic level, the charge transformation implies swapping $p \leftrightarrow n$, $\pi^+ \leftrightarrow \pi^-$, $K^+ \leftrightarrow K^0$, $\bar{K}^0 \leftrightarrow K^-$, etc.

Let us consider nucleus-nucleus ($A+A$) collisions and, for simplicity, assume that both nuclei have an equal number of protons and neutrons. Without referring to a detailed mathematical formalism, charge symmetry means that strong interactions are invariant under the charge transformation of every nucleus and hadron of the initial and final states. For an ensemble of initial states being invariant under the charge transformation, the probabilities of having initial states related by this transformation are equal. This is indeed the case of nucleus-nucleus collisions, for which each nucleus has an equal number of protons and neutrons. Then, the invariance under charge transformation also holds for the final state ensemble, implying that the mean multiplicities of charge-transformation related hadrons, such as K^+ and K^0 as well as \bar{K}^0 and K^- , coincide:

$$\langle K^+ \rangle = \langle K^0 \rangle \text{ and } \langle K^- \rangle = \langle \bar{K}^0 \rangle. \quad (1)$$

Note that since models predict only properties of ensembles of events and not outcomes of single events, we need to consider quantities averaged over the event ensembles. The subject has a vast literature; see, for example Refs. [8–13]. Consequently, the exact isospin symmetry prediction for the charged-to-neutral kaon ratio in nucleus-nucleus collisions with electric charge to baryon number $Q/B = 1/2$ reads²

¹ Units in this paper follow the Particle Data Group (PDG) [3] convention: masses and energies are expressed in MeV (or GeV), whereas momenta in MeV/ c (or GeV/ c). The relative differences are given as the ratio of the difference to the mean.

² The K^0 and \bar{K}^0 states are produced in strong interactions, but they decay through weak interactions. Consequently, in the final state, one observes linear combinations of the latter known as K^0 "short" (K_S^0) and K^0 "long" (K_L^0), where "short" and "long" refer to their weak decay lifetime [3]. By neglecting the small CP violation, the multiplicities corresponding to weak and strong eigenstates are related by $\langle K_S^0 \rangle = \frac{1}{2} \langle K^0 \rangle + \frac{1}{2} \langle \bar{K}^0 \rangle = \langle K_L^0 \rangle$.

$$R_K \equiv \frac{\langle K^+ \rangle + \langle K^- \rangle}{\langle K^0 \rangle + \langle \bar{K}^0 \rangle} = \frac{\langle K^+ \rangle + \langle K^- \rangle}{2\langle K_S^0 \rangle} = 1. \quad (2)$$

This prediction is a reference for experimental testing of the isospin symmetry in hadron production processes. For a more detailed introduction and didactic derivations see Ref. [14].

Here, we report a measurement of the ratio R_K in the 10% most central collisions of argon (Ar) and scandium (Sc) nuclei at center-of-mass energy per nucleon pair equal to $\sqrt{s_{NN}} = 11.9$ GeV. Further on, we compare the NA61/SHINE result with the world data on charged and neutral kaon production in nucleus-nucleus collisions. The results indicate a significant excess of charged over neutral kaon production. This excess cannot be explained by known effects violating the isospin symmetry. This is discussed and demonstrated by comparing experimental results to well-known theoretical approaches, the statistical Hadron Resonance Gas (HRG) [15] and the dynamical Ultrarelativistic Quantum Molecular Dynamics (UrQMD) [16] models. The predictions of models are calculated for reactions corresponding to experimental data, generally with $Q/B < 1/2$. They consider isospin-breaking effects in strong interactions and, importantly, the production and subsequent decays of the ϕ mesons.

Summarizing, the NA61/SHINE Collaboration measures a charged-to-neutral kaon ratio $R_K = 1.184 \pm 0.061$ in Ar+Sc collisions at 11.9 GeV per nucleon pair. This value aligns with previous experimental measurements, albeit their uncertainties are larger. The significance of the isospin symmetry violation beyond the known effects amounts to 4.7σ when all measurements are considered, and uncertainties quoted by the experiments are used. This is the first evidence of an unexplained isospin symmetry violation in hadron production processes.

2 Results

2.1 Production of K mesons in central Ar+Sc collisions at the CERN SPS

The new experimental results presented here have been obtained by the NA61/SHINE fixed-target experiment at the CERN Super Proton Synchrotron [17]. The measurements of K^+ and K^- production in the 10% most central Ar+Sc reactions at $\sqrt{s_{NN}} = 11.9$ GeV have been published elsewhere [18]. The analysis procedure and details of systematic uncertainties are given in Refs. [19, 20]. Here, we present the first measurement of K_S^0 production in nucleus-nucleus collisions from NA61/SHINE. Earlier data from this experiment, on K_S^0 production in $p+C$, π^-+C , π^++C , $\pi^++\text{Be}$, and $p+p$ collisions can be found in Refs. [21–26]. For more details concerning the experimental procedure, see Methods A.

The comparison of the rapidity distribution of K_S^0 mesons to the average of rapidity distributions for K^+ and K^- mesons is presented in Fig. 1. The rapidity y is a relativistic generalization of the particle velocity along the direction of the incoming nuclei. We calculate rapidity in the nucleon-nucleon collision center-of-mass system, and positive y corresponds to the direction of the Ar nucleus.

In the entire range of rapidity covered by the measurement, the averaged charged K mesons yield prevails significantly over the neutral K_S^0 mesons one. To quantify this effect, Table 1 presents the rapidity densities dn/dy of K^+ , K^- and K_S^0 production measured at mid-rapidity ($y \approx 0$). Here, the relative excess of charged mesons is $(18.4 \pm 6.1)\%$. Integration of the two distributions in Fig. 1 over positive rapidity, $y > 0$, gives 4.28 ± 0.13 and 3.22 ± 0.37 for the production rates per collision of $(K^+ + K^-)/2$ and K_S^0 , respectively (total uncertainties are given; the quantities provided for charged K mesons are based on Ref. [18]). The

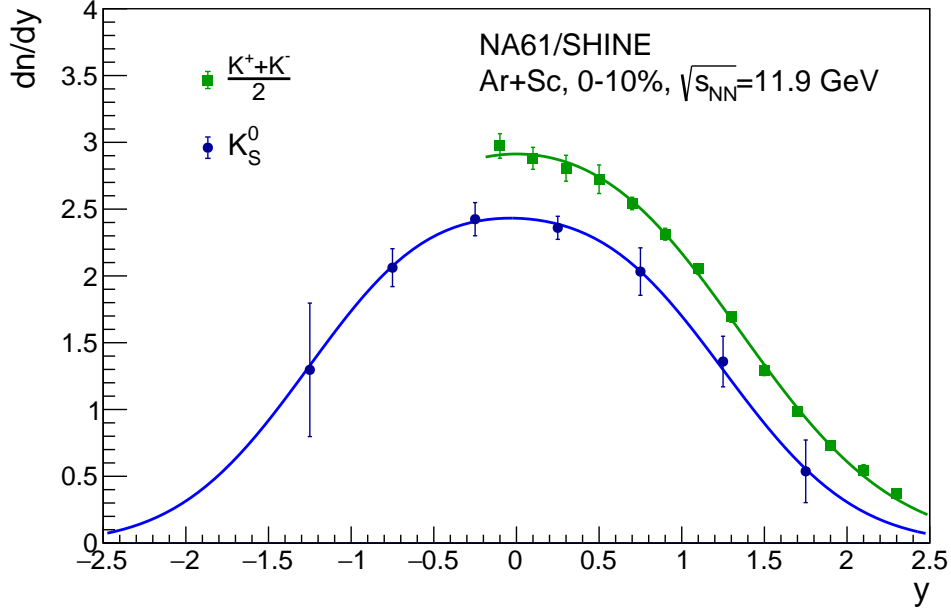


Figure 1: Comparison of rapidity spectrum of neutral (K_S^0) with the averaged spectrum of charged (K^+ and K^-) mesons in the 10% most central Ar+Sc collisions at $\sqrt{s_{NN}} = 11.9$ GeV. Total uncertainties, calculated as the square root of the sum of squared statistical and systematic uncertainties ($\sqrt{\sigma_{stat}^2 + \sigma_{sys}^2}$) are drawn. For charged K mesons, the total uncertainties were calculated separately for positively and negatively charged and then propagated.

resulting difference of 1.06 ± 0.39 corresponds to a surplus of charged (K^+ and K^-) over neutral (K^0 and \bar{K}^0) states equal to 2.12 ± 0.79 at positive rapidity. Under the assumption that the charged-to-neutral ratio would be similar also at negative rapidity, the total excess would amount to 4.2 ± 1.6 additional K^+ or K^- mesons per one central Ar+Sc collision.

A comparison of distributions of K_S^0 with averaged K^+ and K^- mesons as a function of transverse momentum p_T (the momentum component perpendicular to the direction of the incoming nuclei) is shown in Fig. 2. Both distributions are integrated over the rapidity range $0 < y < 2$. The prevalence of charged over neutral K mesons is again evident. The insert in the figure shows the p_T -dependence of the ratio R_K . The corresponding excess of K mesons containing u, \bar{u} over those containing d, \bar{d} quarks and anti-quarks remains in the range 6–33% over the considered range of p_T .

	statistical	systematic	total
$\left(\frac{dn}{dy}\right)_{y\approx 0}(K^+)$	3.732 ± 0.016	± 0.148	± 0.149
$\left(\frac{dn}{dy}\right)_{y\approx 0}(K^-)$	2.029 ± 0.012	± 0.069	± 0.070
$\left(\frac{dn}{dy}\right)_{y\approx 0}(K_S^0)$	2.433 ± 0.027	± 0.102	± 0.106
charged-to-neutral K meson ratio:			
$R_K =$	1.184 ± 0.014	± 0.060	± 0.061

Table 1: Rapidity densities of charged and neutral K mesons produced at mid-rapidity. The measurement was performed in the 10% most central Ar+Sc collisions at $\sqrt{s_{NN}} = 11.9$ GeV, as described in Methods A. The excess of charged over neutral mesons is quantified by the ratio R_K defined in Eq. (2).

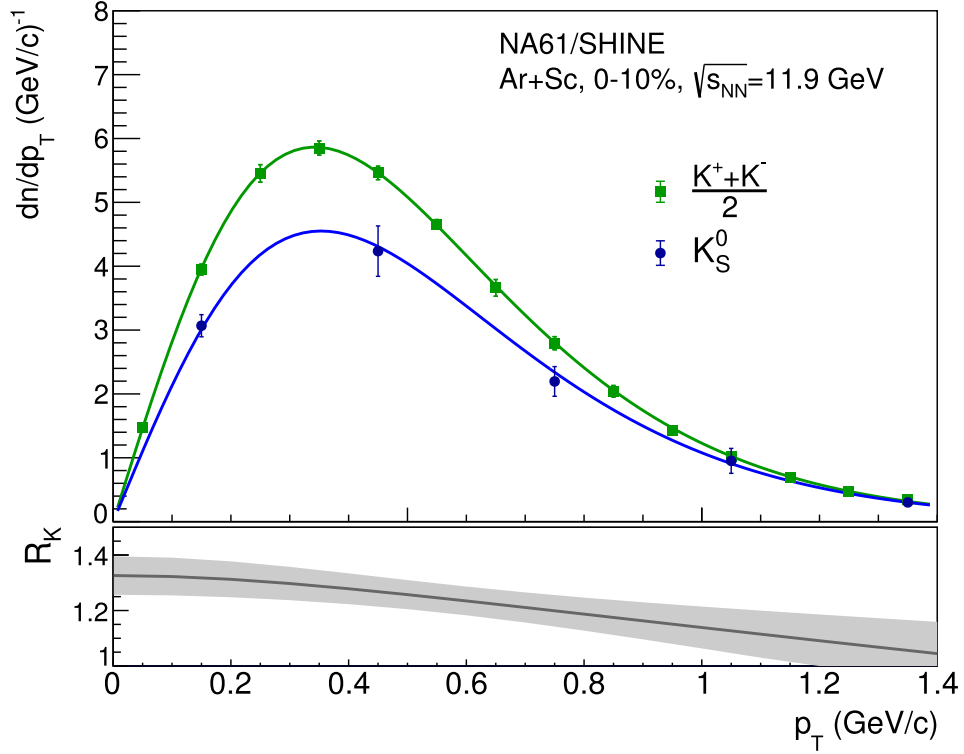


Figure 2: Comparison of transverse momentum spectrum of neutral (K_S^0) with the averaged spectrum of charged (K^+ and K^-) mesons in the 10% most central Ar+Sc collisions at $\sqrt{s_{NN}} = 11.9$ GeV. The bottom panel shows the ratio of the two distributions, as defined in Eq. (2). The meaning of the total uncertainties drawn is the same as in Fig. 1.

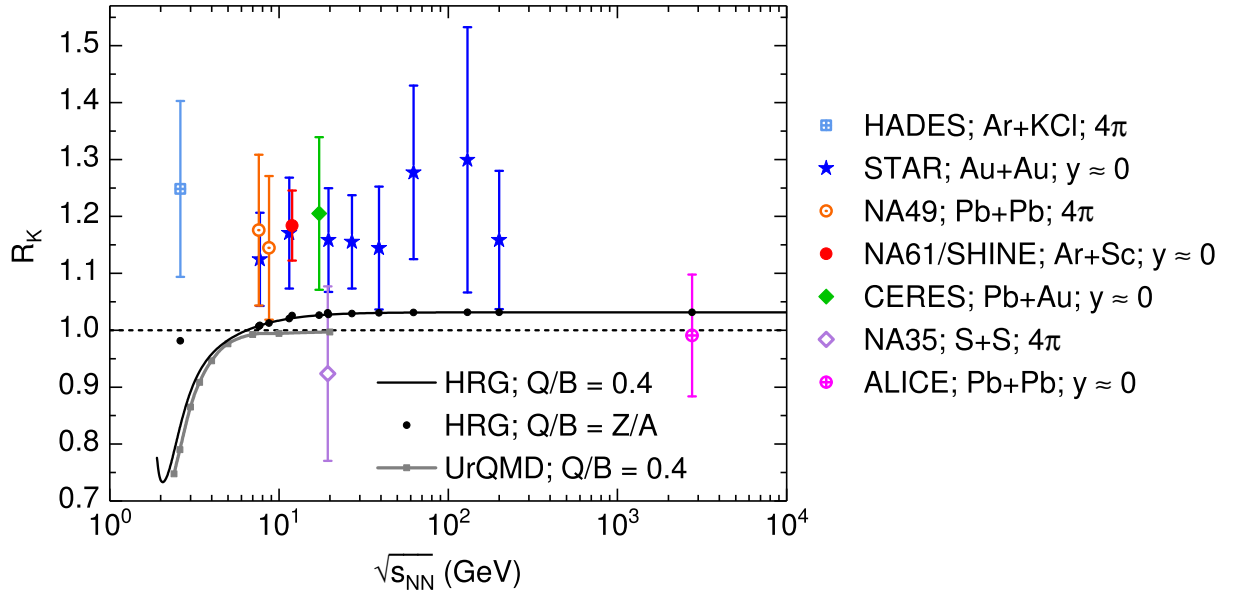


Figure 3: The charged-to-neutral kaon ratio R_K as a function of collision energy. The symbols show the experimental world data with total uncertainties; see Methods B for details. The black line shows the HRG predictions for $Q/B = 0.4$. The black dots indicate the HRG predictions for Q/B values corresponding to the ones in the experiments. For different nuclei, Q/B corresponds to the electric charge over the baryon number of the whole system. The gray squares show UrQMD predictions. See Methods C for details on models.

2.2 Comparison to the world data and models

Figure 3 compares the present measurement of the ratio R_K at mid-rapidity and the world data compiled by us and detailed in Methods B. The experimental results were obtained by CERES [27–29], STAR BES [30, 31], STAR [32–35], ALICE [36, 37], NA35 [38, 39], NA49 [40–42], and HADES [43, 44] experiments. We note that the compilation includes measurements at mid-rapidity and total multiplicities. This may increase the overall spread between the data points. We also note the sizeable uncertainties of the earlier measurements. These probably explain why the aforementioned charged-over-neutral anomaly was never reported as an experimental observation. Despite these uncertainties, a consistent picture emerges in the energy range $2.6 < \sqrt{s_{NN}} < 200$ GeV. The ratio is above one for all experiments except NA35 and ALICE.

Figure 3 also compares the data with the HRG and UrQMD model predictions. The HRG calculations were performed with $Q/B = 0.4$ (solid line) and Q/B values corresponding to collisions studied in the experiments (black dots). The UrQMD results were obtained for central Au+Au collisions. See Methods C for details on the models. The predictions of models agree well with each other but are systematically lower than the experimental data. At energies larger than 10 GeV, the mass difference between charged and neutral kaons, leading to isospin-symmetry breaking (mostly via ϕ -meson decays), increases the R_K ratio by about 0.03. Other isospin-breaking effects can be neglected. The ratio R_K is reduced for collisions with $Q/B < 1/2$, but this is insignificant for energies larger than 10 GeV. At energies lower than 10 GeV, the R_K ratio is significantly more sensitive to the known isospin-breaking effects as well as to the Q/B ratio; see Methods C for more details.

To quantify the measured isospin-symmetry breaking beyond the known effects, the ratio of the measured

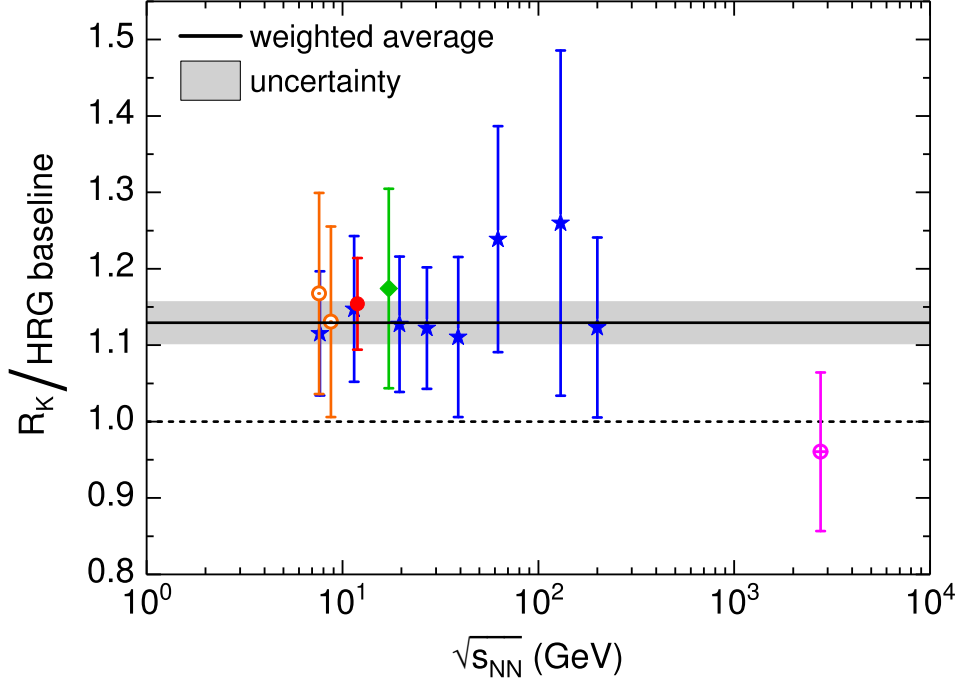


Figure 4: The experimental data for the charged-to-neutral kaon ratio divided by the HRG baseline R_K/R_K^{HRG} as a function of collision energy. The symbols are explained in Fig. 3. The solid black line shows the weighted average of the experimental data, and the shaded area shows the uncertainty of the weighted average.

R_K to the corresponding HRG baseline is shown in Fig. 4. We do not consider the lowest energy data point (HADES) because the known isospin-breaking and $Q/B < 1/2$ effects are significant at the low collision energies; thus, predictions may be model-dependent. We also do not consider the NA35 point because, unlike other measurements, charged kaons were identified by reconstructing their decays, leading to large statistical uncertainties and possible biases. Thus, the number of selected measurements at different collision energies (from SPS to LHC) is 13. Out of them, only one is below unity. No significant dependence of the double ratio on collision energy and nuclear mass number of colliding nuclei is visible.

The weighted average of all double ratios shown in Fig. 4 is 1.129 ± 0.027 , where the uncertainty was calculated using kaon uncertainties reported by experiments. The HRG uncertainties are small and were neglected. The significance of the isospin violation is 4.7σ . The $\chi^2_{min}/dof \approx 0.3$ may indicate either a correlation between results or an overestimation of the uncertainties.

3 Discussion

In the following, we discuss possible effects that may potentially contribute to the violation of isospin symmetry in kaon production.

First, we consider symmetry-breaking effects due to the non-equal bare u and d masses in strong interactions. They are included in the HRG and UrQMD models. Then, we discuss the possible influence related to electromagnetic and weak processes.

- (A) Mass effects within strong interactions. Within QCD, the isospin symmetry is not exact because u and d quark masses are different, ≈ 2.2 and ≈ 4.7 MeV, respectively. The different quark masses lead to different masses of hadrons within the isospin multiplets, particularly different masses of charged and neutral kaons. The ratio R_K can be expanded as a function of the mass difference of the u and d quarks as:

$$R_K = R_K^{(0)} + \frac{m_d - m_u}{\Lambda_{QCD}} R_K^{(1)} + \dots, \quad (3)$$

where $\Lambda_{QCD} \simeq 250$ MeV is the QCD energy scale [4, 5], and $R_K^{(0)}$ is the value of the ratio for the exact isospin symmetry ($m_d = m_u$), being equal to one for $Q/B = 1/2$. The question is whether $R_K^{(1)} + \dots$ terms can reproduce the experimental data. We list below the considered effects and quantify their influence on R_K using the statistical Hadron Resonance Gas model (HRG) [15]. The results are cross-checked with the microscopic transport model, UrQMD [16, 45, 46]. For details, see Methods C.

- (i) Smaller masses of charged kaons than neutral ones, $m_{K^+} = m_{K^-} = 493.7$ MeV and $m_{K^0} = m_{\bar{K}^0} = 497.6$ MeV, lead to an increase of R_K resulting from direct kaon production by about 0.02. This was estimated by removing resonances from the particle list of HRG. We have numerically verified that HRG for $Q/B = 1/2$ and with exact isospin symmetry gives $R_K = 1$, as expected.
 - (ii) Several percent of kaons result from resonance decays [47]. Different kaon masses affect the branching ratios of resonances. The most striking example is $\phi(1020)$ meson, which decays about 1.45 more frequently into charged kaons than neutral ones. This large difference is because the $\phi(1020)$ mass is just above the kaon-kaon thresholds. Including the kaon production from resonance decays increases R_K by about 0.03.
 - (iii) Mass differences of hadrons from other isospin multiplets also break the flavor symmetry and affect R_K . The largest effect comes from the mass difference between proton and neutron, which reduces R_K at the lowest collision energies. At energies larger than 10 GeV, this effect is negligible.
- (B) Electromagnetic processes. Electromagnetic interactions do not obey isospin symmetry because electric charges differ for the quark flavors u and d . The electromagnetic interaction slightly affects the masses of hadrons (for instance, it contributes to render the neutral pion lighter than the charged ones): such effects are taken into account by the HRG, since the physical masses are used. However, the effects mentioned below are not included.
- (i) Electromagnetic decays of hadrons are typically suppressed by a factor $\alpha \simeq 1/137$ compared to strong ones. Consequently, decays that involve the production of virtual photons and their subsequent decay into charged kaons are suppressed by a factor α^2 and thus negligible. Taking into account the charge of the nuclei Z_1 and Z_2 , one would expect an effect of the type $Z_1 Z_2 \alpha^2$, which is not observed in the experimental data – isospin-symmetry breaking for collisions of light and heavy nuclei is similar, see Fig. 4.
 - (ii) The $u\bar{u}$ and $d\bar{d}$ pair creation in strong processes may be affected by electromagnetic interactions. They are different for $u\bar{u}$ and $d\bar{d}$ pairs due to different electric charges of up and $down$ quarks. This leads to a different phase space for their production, favoring $u\bar{u}$ pairs and thus charged kaons. In particular, the quark-gluon effective coupling is enhanced by QED effects due to the attraction among quarks, leading to a larger coupling of gluons to u -quarks than d -quarks [48].

A model of the space-time evolution of the pair creation will be needed to quantify the effect. In addition, the isospin breaking due to the Coulomb potential of highly-charged fireballs formed in heavy-ion collisions is discussed in Ref. [49] within the statistical QGP model. We recall that electromagnetic interactions are expected to modify fusion rates in the Big Bang nucleosynthesis epoch; see, for example, Refs. [50, 51].

- (C) Uncertainties in weak decays. The weak interaction does not obey the isospin symmetry. The mean lifetimes [3] of charged and neutral kaons are $\tau(K^+) = \tau(K^-) = (1.2380 \pm 0.0020) \cdot 10^{-8}$ s and $\tau(K_S^0) = (8.954 \pm 0.004) \cdot 10^{-11}$ s, $\tau(K_L^0) = (5.116 \pm 0.021) \cdot 10^{-8}$ s. The charged kaons are typically measured by reconstructing their trajectories in a detector. Due to the large mean lifetime, the corrections for their losses caused by weak decays are small. In contrast, the neutral K_S^0 kaons are measured by reconstructing their decays into two charged pions. Typically, the corrections for the losses caused by weak decays are large. This is because the decay should be far enough from the interaction point to separate the decay point from the background in high-multiplicity $A+A$ collisions. Assuming that the K_S^0 meson is measurable when the lifetime of a particle in its rest frame is larger than the mean lifetime (typical for NA61/SHINE), one estimates the maximum relative bias of the mean multiplicity, $\Delta(\langle K_S^0 \rangle)/\langle K_S^0 \rangle$, as:

$$\frac{\Delta(\langle K_S^0 \rangle)}{\langle K_S^0 \rangle} = \frac{3 \cdot \sigma(\tau(K_S^0))}{\tau(K_S^0)} \approx 0.0013, \quad (4)$$

where $\sigma(\tau(K_S^0))$ is the uncertainty of the mean K_S^0 lifetime. Thus, the maximum deviation of R_K from unity due to the uncertainty of the mean K_S^0 lifetime is 0.13%.

Finally, we discuss the consequences of having collisions with $Q/B < 1/2$, which corresponds to many experimental results presented in Fig. 3. The third component of isospin equals $|I_z| = |B/2 - Q|$ and therefore the total isospin is limited as $|I_z| \leq I \leq B/2$. The compiled experimental results in nucleus-nucleus collisions correspond to the Q/B ranging from about 0.4 (Pb+Pb and Au+Au collisions) to 0.5 (S+S collisions); see Fig. 3. These limits correspond to the normalized per baryon third component and total isospin $|I_z|/B = 0.1$, $0.1 < I/B < 1/2$ and $|I_z|/B = I/B = 0$, respectively. The non-zero I_z and I for heavier nuclei can affect the charged-to-neutral kaon ratio in two ways:

- (a) The larger fraction of neutrons than protons for heavy nuclei having $|I_z|/B \approx 0.1$ enhances neutral kaon production compared to charged ones and thus reduces R_K . This fact is taken into account by the employed theoretical models that use the physical value for Q/B . The reduction of R_K is significant at low collision energies and is small compared to other effects at energies larger than 10 GeV; see Fig. 3 and Methods C.
- (b) For $|I_z|/B \approx 0.1$, the total isospin is limited by $0.1 \leq I/B \leq 1/2$. Generally, nuclei in the ground state have the lowest possible value of the total isospin [52]. This rule extends to a state of two identical nuclei in the ground state, which, for the considered case, implies $I/B \approx |I_z|/B \approx 0.1$. Thus, a possible dependence of R_K on I and I_z reduces to the dependence on $I = |I_z|$. The latter is discussed above in point (a). The experimental data also allow a rough estimate of the influence of the small but non-zero value of the normalized isospin on the charged-to-neutral kaon ratio. Results for heavy nuclei, $^{208}\text{Pb}+^{208}\text{Pb}$ and $^{197}\text{Au}+^{197}\text{Au}$ ($R_K \approx 1.15$ for $I/B = |I_z|/B \approx 0.1$), are similar to those for intermediate nuclei, $^{40}\text{Ar}+^{45}\text{Sc}$ ($I/B = |I_z|/B \approx 0.04$), and $^{32}\text{S}+^{32}\text{S}$ ($I/B = |I_z|/B = 0$), see Fig. 3. This suggests that the sensitivity of R_K to the $I/B = |I_z|/B$ close to zero ($I/B = |I_z|/B \leq 0.1$) is low. Note, however, that there are large uncertainties in the experimental results.

- (c) In the case of central collisions of heavy nuclei, the charge-to-baryon ratio of the interacting nucleon system (participant nucleons) can be higher than the total proton-to-nucleon ratio in colliding nuclei. This is because protons tend to be distributed closer to the center of a nucleus [53]. However, this effect is expected to be small because the ratio R_K seems independent of the colliding nuclei size. Low-mass nuclei can be described as alpha clusters [54] (clusters of two protons and two neutrons). Thus, if significant, the effect should disappear for collisions of low-mass nuclei, particularly at the lowest collision energies ($\lesssim 4$ GeV), where R_K is sensitive to the small changes of the electric charge to baryon number ratio, Q/B . The data do not support this.

Closing comments on future perspectives of experimental and theoretical efforts are in order here.

- (I) Concerning measurements, reviewing the validity of the past results and confirming them with new high-precision data is important. Systematic results on the collision energy and nuclear mass dependence of the isospin-breaking effect should help us understand its nature. Measurements of the charged-to-neutral kaon ratio in collisions of an equal number of protons and neutrons would reduce uncertainty in its interpretation. The NA61/SHINE experiment plans to perform such measurements for O+O and Mg+Mg collisions [55].
- (II) In connection with the previous point, an interesting experimental test is also possible by considering π^-+C and π^++C interactions [56]. While the ensemble of only one of them is not invariant under charge transformation, the ensemble having an equal number of π^-+C and π^++C interactions is invariant. Thus, for the joint ensemble, the exact charge symmetry predicts $R_K = 1$.
- (III) Kaons play a special role due to their simple isospin structure and easy measurement. This explains why the first results on a large isospin-symmetry breaking in multi-particle production are reported for kaons. Yet, it is important to perform a similar study for other isospin multiplets in the future. For example, using the same methods, we have checked that the (anti-)proton to (anti-)neutron ratio is even less sensitive to the known isospin-symmetry breaking effects and, thus, is predicted to be almost exactly one in nucleus-nucleus collisions with $Q/B = 0.5$ in a broad range of collision energies including the low energies.
- (IV) One can extend the current models by introducing new isospin-breaking processes and fitting their parameters to the data. This can be done either for the quark-gluon processes or the hadron-resonance processes. For example, within the statistical hadronization models, one can introduce the quark fugacity factors for u and d quarks separately [57–59]. This could allow us to make predictions for other hadron ratios but will not explain the origin of the violation.
- (V) The possibility of having a phase of strongly interacting matter with a significant isospin violation was suggested by Pisarski and Wilczek within a linear σ model of QCD [60]. They expect masses of π^0 and η mesons to decrease if the $U_A(1)$ symmetry is effectively restored at temperatures lower than the one of the chiral phase transition. The chiral anomaly [61, 62] could break isospin (especially, it affects the pion isotriplet) but does not affect the charge-to-neutral kaon ratio.
- (VI) Creating Disoriented-Chiral-Condensate (DCC) domains in heavy-ion collisions has been considered for many years [63–65]. They may be signaled by large fluctuations of the charged-to-neutral pion [66] and kaon ratios [67, 68]. A puzzling result on kaon fluctuations was recently reported by ALICE at LHC [69]. Its possible interpretation by the DCC or disoriented-isospin-condensates formation is discussed in Refs. [70, 71]. The considered models for the charged-symmetric ensemble

of collisions predict $R_K = 1$ [72]. The inclusion of isospin-breaking effects in the extended Linear Sigma model [73] was recently discussed in Ref. [74], where through a fit to available experimental masses and decays of light mesons, it is shown that the relative difference between the $u\bar{u}$ and $d\bar{d}$ chiral condensates amounts to 0.02%, implying that only very small deviations from $R_K = 1$ are expected from this effect.

Thus, the presented results on the charged-to-neutral kaon ratio are the first evidence of an unexplained isospin symmetry violation in hadron production processes. Further studies are needed to understand the underlying physics, particularly reducing the experimental uncertainties and quantifying the role of electromagnetic effects. If these steps do not solve the issue, more speculative explanations shall be investigated.

Acknowledgments

We would like to thank the CERN EP, BE, HSE and EN Departments for the strong support of NA61/SHINE. We also gratefully acknowledge discussions with Claudia Ahdida, Wojciech Broniowski, Marco van Leeuwen, Krzysztof Golec-Biernat, Stanisław Mrówczyński, Owe Philippsen, Rob Pisarski, Krishna Rajagopal, Jan Rafelski, Jan Steinheimer, Leonardo Tinti, and Volodymyr Vovchenko for fruitful discussions and comments at various stages of the preparation of this article.

This work was supported by the Hungarian Scientific Research Fund (grant NKFIH 138136/137812/138152 and TKP2021-NKTA-64), the Polish Ministry of Science and Higher Education (DIR/WK/2016/2017/10-1, WUT ID-UB), the National Science Centre Poland (grants 2014/14/E/ST2/00018, 2016/21/D/ST2/01983, 2017/25/N/ST2/02575, 2018/29/N/ST2/02595, 2018/30/A/ST2/00226, 2018/31/G/ST2/03910, 2019/33/B/ST2/00613, 2020/39/O/ST2/00277), the Norwegian Financial Mechanism 2014–2021 (grant 2019/34/H/ST2/00585), the Polish Minister of Education and Science (contract No. 2021/WK/10), the Internationalisation of the Jan Kochanowski University Doctoral School of the Polish Academy Agency for Academic Exchange NAWA STER no. BPI/STE/2023/1/00014, the European Union’s Horizon 2020 research and innovation programme under grant agreement No. 871072, the Ministry of Education, Culture, Sports, Science and Technology, Japan, Grant-in-Aid for Scientific Research (grants 18071005, 19034011, 19740162, 20740160 and 20039012,22H04943), the German Research Foundation DFG (grants GA 1480/8-1 and project 426579465), the Bulgarian Ministry of Education and Science within the National Roadmap for Research Infrastructures 2020–2027, contract No. D01-374/18.12.2020, Serbian Ministry of Science, Technological Development and Innovation (grant OI171002), Swiss Nationalfonds Foundation (grant 200020117913/1), ETH Research Grant TH-01 07-3, National Science Foundation grant PHY-2013228 and the Fermi National Accelerator Laboratory (Fermilab), a U.S. Department of Energy, Office of Science, HEP User Facility managed by Fermi Research Alliance, LLC (FRA), acting under Contract No. DE-AC02-07CH11359 and the IN2P3-CNRS (France), the German Research Foundation grants GA1480/8-1, and the Alexander von Humboldt Foundation.

The data used in this article were collected before February 2022.

References

- [1] H. Fritzsch, M. Gell-Mann, and H. Leutwyler, “Advantages of the color octet gluon picture,” *Phys. Lett. B* **47** (1973) 365–368.
- [2] W. Heisenberg, “On the structure of atomic nuclei,” *Z. Phys.* **77** (1932) 1–11.
- [3] S. Navas *et al.*, [Particle Data Group Collab.], “Review of Particle Physics,” *Phys. Rev. D* **110** (2024) 030001.
- [4] J. L. Kneur and A. Neveu, “ $\Lambda_{\overline{\text{MS}}}^{\text{QCD}}$ from renormalization group optimized perturbation,” *Phys. Rev. D* **85** (2012) 014005, arXiv:1108.3501 [hep-ph].
- [5] A. Deur, S. J. Brodsky, and G. F. de Téramond, “The QCD running coupling,” *Nucl. Phys.* **90** (2016) 1, arXiv:1604.08082 [hep-ph].
- [6] M. R. Pennington, “Swimming with Quarks,” *J. Phys. Conf. Ser.* **18** (2005) 1–73, arXiv:hep-ph/0504262.
- [7] J. M. Alarcón, J. Martin Camalich, and J. A. Oller, “The chiral representation of the πN scattering amplitude and the pion-nucleon sigma term,” *Phys. Rev. D* **85** (2012) 051503, arXiv:1110.3797 [hep-ph].
- [8] I. Shmushkevich, *Dokl. Akad. Nauk SSSR* **103** (1955) 235.
- [9] N. Dushin and I. Shmushkevich, *Dokl. Akad. Nauk SSSR* **106** (1956) 801.
- [10] G. Pinski, A. J. MacFarlane, and G. Sudarshan, “Shmushkevich’s Method for a Charge-Independent Theory,” *Phys. Rev.* **140** (1965) B1045.
- [11] C. G. Wohl, “Isospin relations by counting,” *Am. J. Phys.* **50** (1982) 748–753.
- [12] P. B. Pal, “An Introductory Course of Particle Physics,” CRC Press, Taylor & Francis Group (2015).
- [13] M. Gazdzicki and O. Hansen, “Hadron production in nucleon-nucleon collisions at 200 GeV/c – A Compilation,” *Nucl. Phys. A* **528** (1991) 754–770.
- [14] W. Brylinski, M. Gazdzicki, F. Giacosa, M. Gorenstein, R. Poberezhnyuk, S. Samanta, and H. Stroebele, “Large isospin symmetry breaking in kaon production at high energies,” arXiv:2312.07176 [nucl-th].
- [15] V. Vovchenko and H. Stoecker, “THERMAL-FIST: A package for heavy-ion collisions and hadronic equation of state,” *Comput. Phys. Commun.* **244** (2019) 295–310, arXiv:1901.05249 [nucl-th].
- [16] M. Bleicher *et al.*, “Relativistic hadron-hadron collisions in the ultra-relativistic quantum molecular dynamics model,” *J. Phys. G* **25** (1999) 1859–1896, arXiv:hep-ph/9909407.
- [17] N. Abgrall *et al.*, [NA61/SHINE Collab.], “NA61/SHINE facility at the CERN SPS: beams and detector system,” *J. Inst.* **9** (2014) P06005, arXiv:1401.4699.
- [18] H. Adhikary *et al.*, [NA61/SHINE Collab.], “Measurements of π^\pm , K^\pm , p and \bar{p} spectra in $^{40}\text{Ar}+^{45}\text{Sc}$ collisions at 13A to 150A GeV/c,” *Eur. Phys. J. C* **84** no. 4, (2024) 416, arXiv:2308.16683 [nucl-ex].

- [19] M. Lewicki, "Charged hadron production in central Ar+Sc collisions at the CERN SPS," PhD thesis CERN-THESIS-2020-349, University of Wrocław, 2020. <https://cds.cern.ch/record/2772291>.
- [20] P. Podlaski, "Study of charged hadron production with tof-dE/dx identification method in central Ar+Sc collisions in NA61/SHINE experiment at CERN," PhD thesis CERN-THESIS-2021-250, University of Warsaw, 2021. <https://cds.cern.ch/record/2799198>.
- [21] N. Abgrall *et al.*, [NA61/SHINE Collab.], "Measurements of π^\pm , K^\pm , K_S^0 , Λ and proton production in proton-carbon interactions at 31 GeV/c with the NA61/SHINE spectrometer at the CERN SPS," *Eur. Phys. J. C* **76** no. 2, (2016) 84, arXiv:1510.02703 [hep-ex].
- [22] H. Adhikary *et al.*, [NA61/SHINE Collab.], "Measurements of K_S^0 , Λ , and $\bar{\Lambda}$ production in 120 GeV/c p+C interactions," *Phys. Rev. D* **107** no. 7, (2023) 072004, arXiv:2211.00183 [hep-ex].
- [23] H. Adhikary *et al.*, [NA61/SHINE Collab.], "Measurement of hadron production in π^- -C interactions at 158 and 350 GeV/c with NA61/SHINE at the CERN SPS," *Phys. Rev. D* **107** no. 6, (2023) 062004, arXiv:2209.10561 [nucl-ex].
- [24] A. Aduszkiewicz *et al.*, [NA61/SHINE Collab.], "Measurements of hadron production in π^+ +C and π^+ +Be interactions at 60 GeV/c," *Phys. Rev. D* **100** no. 11, (2019) 112004, arXiv:1909.06294 [hep-ex].
- [25] A. Acharya *et al.*, [NA61/SHINE Collab.], " K_S^0 meson production in inelastic $p+p$ interactions at 158 GeV/c beam momentum measured by NA61/SHINE at the CERN SPS," *Eur. Phys. J. C* **82** no. 1, (2022) 96, arXiv:2106.07535 [hep-ex].
- [26] N. Abgrall *et al.*, [NA61/SHINE Collab.], " K_S^0 meson production in inelastic $p+p$ interactions at 31, 40 and 80 GeV/c beam momentum measured by NA61/SHINE at the CERN SPS," *Eur. Phys. J. C* **84** no. 8, (2024) 820, arXiv:2402.17025 [hep-ex].
- [27] M. Kaliský, "Reconstruction of charged kaons in the three pion decay channel in Pb+Au 158 AGeV collisions by the CERES experiment," PhD thesis CERN-THESIS-2007-132, Technical University of Darmstadt, 2007. <https://cds.cern.ch/record/1497739>.
- [28] S. Radomski, [CERES Collab.], "CERES measurement of strangeness production at top SPS energy," *J. Phys. G* **35** (2008) 044003.
- [29] S. Radomski, "Neutral strange particle production at top SPS energy measured by the CERES experiment," PhD thesis CERN-THESIS-2006-117, Technical University of Darmstadt, 2006. <http://cds.cern.ch/record/1497741>.
- [30] L. Adamczyk *et al.*, [STAR Collab.], "Bulk properties of the medium produced in relativistic heavy-ion collisions from the beam energy scan program," *Phys. Rev. C* **96** no. 4, (2017) 044904, arXiv:1701.07065 [nucl-ex].
- [31] J. Adam *et al.*, [STAR Collab.], "Strange hadron production in Au+Au collisions at $\sqrt{s_{NN}} = 7.7, 11.5, 19.6, 27, \text{ and } 39$ GeV," *Phys. Rev. C* **102** no. 3, (2020) 034909, arXiv:1906.03732 [nucl-ex].
- [32] C. Adler *et al.*, [STAR Collab.], "Kaon production and kaon to pion ratio in Au+Au collisions at $\sqrt{s_{NN}} = 130$ GeV," *Phys. Lett. B* **595** (2004) 143–150, arXiv:nucl-ex/0206008.

- [33] B. I. Abelev *et al.*, [STAR Collab.], “Systematic measurements of identified particle spectra in pp , $d+Au$ and $Au+Au$ collisions at the STAR detector,” *Phys. Rev. C* **79** (2009) 034909, arXiv:0808.2041 [nucl-ex].
- [34] M. M. Aggarwal *et al.*, [STAR Collab.], “Strange and multistrange particle production in $Au+Au$ collisions at $\sqrt{s_{NN}} = 62.4$ GeV,” *Phys. Rev. C* **83** (2011) 024901, arXiv:1010.0142 [nucl-ex]. [Erratum: *Phys.Rev.C* 107, 049903 (2023)].
- [35] G. Agakishiev *et al.*, [STAR Collab.], “Strangeness Enhancement in $Cu-Cu$ and $Au-Au$ Collisions at $\sqrt{s_{NN}} = 200$ GeV,” *Phys. Rev. Lett.* **108** (2012) 072301, arXiv:1107.2955 [nucl-ex].
- [36] B. Abelev *et al.*, [ALICE Collab.], “Centrality dependence of π , K , p production in $Pb-Pb$ collisions at $\sqrt{s_{NN}} = 2.76$ TeV,” *Phys. Rev. C* **88** (2013) 044910, arXiv:1303.0737 [hep-ex].
- [37] B. Abelev *et al.*, [ALICE Collab.], “ K_S^0 and Λ Production in $Pb-Pb$ Collisions at $\sqrt{s_{NN}} = 2.76$ TeV,” *Phys. Rev. Lett.* **111** (2013) 222301, arXiv:1307.5530 [nucl-ex].
- [38] J. Baechler *et al.*, [NA35 Collab.], “Production of charged kaons in proton-nucleus and nucleus-nucleus collisions at 200 GeV/nucleon,” *Z. Phys. C* **58** (1993) 367–374.
- [39] T. Alber *et al.*, [NA35 Collab.], “Strange particle production in nuclear collisions at 200 GeV per nucleon,” *Z. Phys. C* **64** (1994) 195–207.
- [40] C. Alt *et al.*, [NA49 Collab.], “Pion and kaon production in central $Pb+Pb$ collisions at 20A and 30A GeV: Evidence for the onset of deconfinement,” *Phys. Rev. C* **77** (2008) 024903, arXiv:0710.0118 [nucl-ex].
- [41] S. V. Afanasiev *et al.*, [NA49 Collab.], “Energy dependence of pion and kaon production in central $Pb+Pb$ collisions,” *Phys. Rev. C* **66** (2002) 054902, arXiv:nucl-ex/0205002.
- [42] C. Strabel, “Energieabhängigkeit der K_S^0 -Produktion in zentralen $Pb+Pb$ Reaktionen,” MSc thesis NA49-PUBLIC, Johann Wolfgang Goethe-Universität, 2006. <https://edms.cern.ch/document/2958534/1>.
- [43] G. Agakishiev *et al.*, [HADES Collab.], “ ϕ decay: A relevant source for K^- production at energies available at the GSI Schwerionen-Synchrotron (SIS)?,” *Phys. Rev. C* **80** (2009) 025209, arXiv:0902.3487 [nucl-ex].
- [44] G. Agakishiev *et al.*, [HADES Collab.], “In-medium effects on K^0 mesons in relativistic heavy-ion collisions,” *Phys. Rev. C* **82** (2010) 044907, arXiv:1004.3881 [nucl-ex].
- [45] S. A. Bass *et al.*, “Microscopic models for ultrarelativistic heavy ion collisions,” *Prog. Part. Nucl. Phys.* **41** (1998) 255–369, arXiv:nucl-th/9803035.
- [46] M. Bleicher and E. Bratkovskaya, “Modelling relativistic heavy-ion collisions with dynamical transport approaches,” *Prog. Part. Nucl. Phys.* **122** (2022) 103920.
- [47] F. Becattini, J. Manninen, and M. Gaździcki, “Energy and system size dependence of chemical freeze-out in relativistic nuclear collisions,” *Phys. Rev. C* **73** (2006) 044905, arXiv:hep-ph/0511092 [hep-ph].
- [48] T. Goldman, K. R. Maltman, and G. J. Stephenson, “The finite QED correction to the quark-gluon vertex,” *Phys. Lett. B* **228** (1989) 396–400.

- [49] J. Letessier and J. Rafelski, “Chemical nonequilibrium in high-energy nuclear collisions,” *J. Phys. G* **25** (1999) 295–309, arXiv:hep-ph/9810332.
- [50] E. E. Salpeter, “Electron Screening and Thermonuclear Reactions,” *Austral. J. Phys.* **7** (1954) 373–388.
- [51] C. Grayson, C. T. Yang, M. Formanek, and J. Rafelski, “Self-consistent strong screening applied to thermonuclear reactions,” arXiv:2406.13055 [nucl-th].
- [52] S. M. Lenzi and M. A. Bentley, “Test of Isospin Symmetry Along the $N = Z$ Line,” *Lect. Notes Phys.* **764** (2009) 57–98.
- [53] M. Thiel, C. Sfonti, J. Piekarewicz, C. J. Horowitz, and M. Vanderhaeghen, “Neutron skins of atomic nuclei: per aspera ad astra,” *J. Phys. G* **46** no. 9, (2019) 093003, arXiv:1904.12269 [nucl-ex].
- [54] T. Otsuka, T. Abe, T. Yoshida, Y. Tsunoda, N. Shimizu, N. Itagaki, Y. Utsuno, J. Vary, P. Maris, and H. Ueno, “ α -Clustering in atomic nuclei from first principles with statistical learning and the Hoyle state character,” *Nature Commun.* **13** no. 1, (2022) 2234.
- [55] H. Adhikary *et al.*, [NA61/SHINE Collab.], “Addendum to the NA61/SHINE Proposal: Request for light ions beams in Run 4,” Tech. Rep. CERN-SPSC-2023-022, SPSC-P-330-ADD-14, CERN, Geneva, 2023. <https://cds.cern.ch/record/2867952>.
- [56] H. Adhikary *et al.*, [NA61/SHINE Collab.], “Memorandum requesting use of the allocated test beam for data-taking on $\pi^+ + C$ and $\pi^- + C$ interactions at 158 GeV/c,” Tech. Rep. CERN-SPSC-2024-022, SPSC-M-797, CERN, Geneva, 2024. <https://cds.cern.ch/record/2907307>.
- [57] M. Petráň, J. Letessier, V. Petráček, and J. Rafelski, “Hadron production and quark-gluon plasma hadronization in Pb-Pb collisions at $\sqrt{s_{NN}} = 2.76$ TeV,” *Phys. Rev. C* **88** no. 3, (2013) 034907, arXiv:1303.2098 [hep-ph].
- [58] J. Rafelski and M. Petráň, “Universal QGP Hadronization Conditions at RHIC and LHC,” *EPJ Web Conf.* **78** (2014) 06004, arXiv:1406.1871 [nucl-th].
- [59] J. Rafelski and M. Petran, “QCD Phase Transition Studied by Means of Hadron Production,” *Phys. Part. Nucl.* **46** no. 5, (2015) 748–755, arXiv:2212.13302 [hep-ph].
- [60] R. D. Pisarski and F. Wilczek, “Remarks on the chiral phase transition in chromodynamics,” *Phys. Rev. D* **29** (1984) 338–341.
- [61] F. Giacosa, A. Koenigstein, and R. D. Pisarski, “How the axial anomaly controls flavor mixing among mesons,” *Phys. Rev. D* **97** no. 9, (2018) 091901, arXiv:1709.07454 [hep-ph].
- [62] F. Giacosa, S. Jafarzade, and R. D. Pisarski, “Anomalous interactions between mesons with nonzero spin and glueballs,” *Phys. Rev. D* **109** no. 7, (2024) L071502, arXiv:2309.00086 [hep-ph].
- [63] A. A. Anselm and M. G. Ryskin, “Production of classical pion field in heavy ion high energy collisions,” *Phys. Lett. B* **266** (1991) 482–484.
- [64] J.-P. Blaizot and A. Krzywicki, “Soft pion emission in high-energy heavy-ion collisions,” *Phys. Rev. D* **46** (1992) 246–251.
- [65] K. Rajagopal and F. Wilczek, “Emergence of coherent long wavelength oscillations after a quench: application to QCD,” *Nucl. Phys. B* **404** (1993) 577–589, arXiv:hep-ph/9303281.

- [66] J. D. Bjorken, K. L. Kowalski, and C. C. Taylor, “Observing Disoriented Chiral Condensates,” in *Workshop on Physics at Current Accelerators and the Supercollider*. 9, 1993. arXiv:hep-ph/9309235.
- [67] J. Schaffner-Bielich and J. Randrup, “Disoriented chiral condensate dynamics with the SU(3) linear sigma model,” *Phys. Rev. C* **59** (1999) 3329–3342, arXiv:nuc1-th/9812032.
- [68] S. Gavin and J. I. Kapusta, “Kaon and pion fluctuations from small disoriented chiral condensates,” *Phys. Rev. C* **65** (2002) 054910, arXiv:nuc1-th/0112083.
- [69] S. Acharya *et al.*, [ALICE Collab.], “Neutral to charged kaon yield fluctuations in Pb – Pb collisions at $\sqrt{s_{NN}} = 2.76$ TeV,” *Phys. Lett. B* **832** (2022) 137242, arXiv:2112.09482 [nucl-ex].
- [70] J. I. Kapusta, S. Pratt, and M. Singh, “Confronting anomalous kaon correlations measured in Pb-Pb collisions at $\sqrt{s_{NN}} = 2.76$ TeV,” *Phys. Rev. C* **107** no. 1, (2023) 014913, arXiv:2210.03257 [hep-ph].
- [71] J. I. Kapusta, S. Pratt, and M. Singh, “Disoriented isospin condensates may be the source of anomalous kaon correlations measured in Pb-Pb collisions at $\sqrt{s_{NN}} = 2.76$ TeV,” *Phys. Rev. C* **109** no. 3, (2024) L031902, arXiv:2306.13280 [hep-ph].
- [72] M. Singh *et al.*, “Disoriented Isospin Condensates as source of anomalous kaon correlations at LHC,” in *21st International Conference on Strangeness in Quark Matter (SQM 2024)*. 2024. <https://indico.in2p3.fr/event/29792/contributions/137151>.
- [73] D. Parganlija, P. Kovács, G. Wolf, F. Giacosa, and D. H. Rischke, “Meson vacuum phenomenology in a three-flavor linear sigma model with (axial-)vector mesons,” *Phys. Rev. D* **87** no. 1, (2013) 014011, arXiv:1208.0585 [hep-ph].
- [74] P. Kovács, G. Wolf, N. Weickgenannt, and D. H. Rischke, “Phenomenology of isospin-symmetry breaking with vector mesons,” *Phys. Rev. D* **109** no. 9, (2024) 096007, arXiv:2401.04527 [hep-ph].
- [75] W. Bryliński, “Study of K_S^0 meson production in central Ar+Sc collisions at SPS energies,” PhD thesis CERN-THESIS-2023-404, Warsaw University of Technology, 2023. <https://cds.cern.ch/record/2907562>.
- [76] K. Werner, “The hadronic interaction model EPOS,” *Nucl. Phys. Proc. Suppl.* **175-176** (2008) 81–87.
- [77] R. Brun, R. Hagelberg, M. Hansroul, and J. C. Lassalle, “Simulation Program for Particle Physics Experiments, GEANT: User Guide and Reference Manual,” Tech. Rep. CERN-DD-78-2-REV, CERN-DD-78-2, CERN, Geneva, 1978. <https://cds.cern.ch/record/118715>.
- [78] J. Adamczewski-Musch *et al.*, [HADES Collab.], “Deep sub-threshold ϕ production in Au+Au collisions,” *Phys. Lett. B* **778** (2018) 403–407, arXiv:1703.08418 [nucl-ex].
- [79] J. Adamczewski-Musch *et al.*, [HADES Collab.], “Sub-threshold production of K_S^0 mesons and Λ hyperons in Au+Au collisions at $\sqrt{s_{NN}} = 2.4$ GeV,” *Phys. Lett. B* **793** (2019) 457–463, arXiv:1812.07304 [nucl-ex].
- [80] P. Gasik *et al.*, [FOPI Collab.], “Strange meson production in Al+Al collisions at 1.9 A GeV,” *Eur. Phys. J. A* **52** no. 6, (2016) 177, arXiv:1512.06988 [nucl-ex].

- [81] X. Lopez *et al.*, [FOPI Collab.], “Measurement of $K^*(892)^0$ and K^0 mesons in Al+Al collisions at 1.9A GeV,” *Phys. Rev. C* **81** (2010) 061902, arXiv:1006.1905 [nucl-ex].
- [82] M. Gaździcki and D. Röhrich, “Strangeness in nuclear collisions,” *Z. Phys. C* **71** (1996) 55–64, arXiv:hep-ex/9607004.
- [83] D. Röhrich *et al.*, [NA35 Collab.], “Hadron Production in S+Ag and S+Au Collisions at 200 GeV/Nucleon,” *Nucl. Phys. A* **566** (1994) 35C–44C.
- [84] C. Patrignani *et al.*, [Particle Data Group Collab.], “Review of Particle Physics,” *Chin. Phys. C* **40** no. 10, (2016) 100001.
- [85] P. Braun-Munzinger, J. Cleymans, H. Oeschler, and K. Redlich, “Maximum relative strangeness content in heavy-ion collisions around 30 A GeV,” *Nucl. Phys. A* **697** (2002) 902–912, arXiv:hep-ph/0106066.
- [86] H. Oeschler, J. Cleymans, B. Hippolyte, K. Redlich, and N. Sharma, “Thermal Model Description of Collisions of Small Nuclei,” arXiv:1603.09553 [hep-ph].
- [87] J. Rafelski, “Melting hadrons, boiling quarks,” *Eur. Phys. J. A* **51** no. 9, (2015) 114, arXiv:1508.03260 [nucl-th].
- [88] R. V. Poberezhnyuk, V. Vovchenko, A. Motornenko, M. I. Gorenstein, and H. Stöcker, “Chemical freeze-out conditions and fluctuations of conserved charges in heavy-ion collisions within quantum van der Waals model,” *Phys. Rev. C* **100** no. 5, (2019) 054904, arXiv:1906.01954 [hep-ph].
- [89] V. Vovchenko, M. I. Gorenstein, and H. Stoecker, “Finite resonance widths influence the thermal-model description of hadron yields,” *Phys. Rev. C* **98** no. 3, (2018) 034906, arXiv:1807.02079 [nucl-th].
- [90] J. Cleymans, H. Oeschler, K. Redlich, and S. Wheaton, “Comparison of chemical freeze-out criteria in heavy-ion collisions,” *Phys. Rev. C* **73** (2006) 034905, arXiv:hep-ph/0511094.
- [91] B. Andersson, G. Gustafson, and B. Söderberg, “A General Model for Jet Fragmentation,” *Z. Phys. C* **20** (1983) 317.

Methods

A. Experimental procedure

Experimental setup. The SPS Heavy Ion and Neutrino Experiment (SHINE) is a fixed-target detector operating at the CERN Super Proton Synchrotron (SPS). It is a multi-purpose spectrometer optimized to study hadron production in various collisions (hadron-proton, hadron-nucleus, and nucleus-nucleus). The detection setup used for the measurements reported here is described below. Its details and a description of the detector performance can be found in Ref. [17].

The beamline is equipped with an array of beam detectors upstream and downstream of the target, used to identify and measure the trajectory of the beam particles and trigger the spectrometer data acquisition. The tracking devices of the NA61/SHINE spectrometer are Time Projection Chambers (TPCs). Two Vertex TPCs are placed inside a magnetic field. Two large-volume Main TPCs measure the charged particle trajectories downstream of the 4.5 Tm magnetic field. The latter provides the bending power for a precise determination of particle momenta. The information about the energy losses (dE/dx) of the charged particles in the TPCs, together with Time-of-Flight (ToF) measurements, allows for particle identification in a wide momentum range. The most downstream detector on the beamline is the Projectile Spectator Detector (PSD). It measures the energy of the “spectator” remnant of the projectile nucleus, closely related to the collision centrality in nucleus-nucleus reactions.

Physics objects. This article compares the production of charged and neutral K mesons in Ar+Sc collisions at a center-of-mass energy per nucleon pair of 11.9 GeV. The $^{40}_{18}\text{Ar}$ beam had a momentum of $75A \text{ GeV}/c$. The stationary target consisted of six $^{45}_{21}\text{Sc}$ plates, with a total thickness of 6 mm.

A detailed account on the extraction of charged (K^+ , K^-) yields can be found in Ref. [18]. Only the neutral K^0_S mesons are considered in the present analysis. They can be detected via their weak decay into two charged pions ($K^0_S \rightarrow \pi^+\pi^-$). The mean lifetime ($c\tau$) for this decay is 2.7 cm. A detailed presentation of the K^0_S analysis procedure and systematic uncertainties can be found in Ref. [75].

Analysis. Before analyzing K^0_S mesons, the recorded Ar+Sc collision data undergo event and track selection procedures. Event selection uses information from the beam detectors to ensure the quality of the measured beam trajectory. It rejects events with more than one beam-target interaction during the trigger-time window. It also reduces the background from off-target interactions based on information about the quality of the main interaction vertex. Finally, it selects the 10% most central collisions using the information from the PSD. This is realized by selecting the 10% lowest energy deposits from the spectator remnant of the Ar nucleus. The total number of recorded collisions (events) was $2.77 \cdot 10^6$, from which $1.03 \cdot 10^6$ (37%) remained after all cuts. For more details, especially the centrality selection, see Ref. [18].

The next step is reconstructing the charged particle tracks in the TPCs. Pattern recognition algorithms combine space points recorded in the TPCs into tracks. Their curvature and the magnetic field are used to compute the momenta of the corresponding particles. The minimum number of reconstructed space points in the VTPCs must be more than 10, and the computed momenta must be larger than $400 \text{ MeV}/c$ (in the laboratory frame). The latter selection excludes a large fraction of low-momentum electrons from the analysis. The known positions of the target and the most probable intersection point of measured tracks define the position of the primary vertex.

K^0_S reconstruction. Unlike the charged particles, the neutral K mesons do not leave a measurable track

in the detectors. They are measured by reconstructing their oppositely charged decay products (daughter particles). The two-body decays of K_S^0 create characteristic V -shaped particle pairs originating at the decay vertex. This topology is called V^0 . It is searched with a dedicated V^0 -finder algorithm that looks for track pairs of particles with opposite charges. These track pairs are extrapolated backwards until their mutual distance of the closest approach is reached. If this distance is smaller than a given limit value, the track pair becomes a V^0 candidate with its origin at the decay vertex.

Two further cuts are placed on the track pairs. The first cut imposes a minimum value on the angle between the direction of the line joining the primary and decay vertices and the direction given by the vector sum of the momenta of the decay daughters. The second condition requires a minimum distance between the primary and decay vertex (a minimum length of the decaying particle). The corresponding cut requirements depend on K_S^0 rapidity and are listed in Extended Data Table 4. Starting with the approximate decay point, a V^0 -fitter program optimizes the decay point position and the momenta of the decay daughters. Assuming that the daughter particles are pions, it is straightforward to reconstruct the invariant mass of the decaying particle (the invariant mass is defined as $m_{inv} = \sqrt{(\sum E_i)^2 - (\sum \vec{p}_i)^2}$, where E_i are the energies of the decay products, \vec{p}_i are their momenta, and $c \equiv 1$ is assumed).

The invariant mass distribution of V^0 candidates is populated by K_S^0 and Λ decays, photon conversion in some detector material, and spurious particle crossings. A K_S^0 signal will appear as a peak on a slowly varying background. For a double-differential K_S^0 analysis, the momentum space was divided into seven rapidity bins ranging from -1.5 to 2 and nine transverse-momentum bins ranging from 0 to 2.7 GeV/ c . The raw number of K_S^0 in a given kinematic bin is obtained from fits of appropriate signal and background functions to the invariant mass distribution of the corresponding V^0 candidates. The fitted signal function is taken as a Lorentzian, and the background function is a third-order Chebychev polynomial. The integral of the signal function divided by the bin width is equal to the raw (uncorrected) number of the reconstructed K_S^0 in a given kinematic bin. Two typical invariant mass distributions with signal and background fits are shown in Extended Data Fig. 5.

Corrections. To correct the results for losses due to detection and data processing inefficiencies, detailed Monte Carlo simulations were performed. These simulations comprised Ar+Sc collisions generated by the EPOS model [76], and particles propagated in the NA61/SHINE detector using the GEANT framework [77]. The charged particle tracks were reconstructed and analyzed using the same software as used for the experimental data. The branching ratio of K_S^0 decays was considered in the GEANT framework. The final output of the simulation consisted of reconstructed K_S^0 multiplicities. The ratio of the simulated and reconstructed numbers of K_S^0 was used as a correction factor in each y - p_T bin.

Systematic uncertainties of the measured data points were estimated by comparing the results of the entire analysis (including Monte Carlo simulations and corrections) obtained with varying cut values. The reliability of the V^0 reconstruction and K_S^0 fitting procedures can be scrutinized by studying the K_S^0 lifetime. Extended Data Fig. 6 shows the computed mean lifetime of K_S^0 in seven rapidity bins. Good agreement with the average value provided by the PDG [3] is observed.

Transverse momentum distributions. The distributions shown in Extended Data Fig. 7 represent the final results of the K_S^0 analysis. The K_S^0 yields are shown as a function of transverse momentum in seven bins of rapidity. The data points are fitted with the function:

$$f(p_T) = A \cdot p_T \cdot \exp\left(-\frac{\sqrt{p_T^2 + m_0^2}}{T}\right), \quad (5)$$

in which A is a normalisation factor, T is the inverse slope parameter, and m_0 is the K_S^0 mass taken from Ref. [3]. The formula assumes $c \equiv 1$ for simplicity. The fit functions are plotted as red curves, and the inverse slope parameters obtained from the fits are reported in the figure legends.

The transverse momentum distributions of charged and neutral K mesons drawn in Fig. 2 (of the main text) are also fitted with the function defined by Eq. (5). The bottom panel of the figure presents the ratio of the two fitted curves, with its uncertainty band obtained by the propagation of the uncertainties of the fitted parameters.

Rapidity distribution. The final K_S^0 yields in each bin of rapidity were obtained as the integrals of the curves fitted to the respective transverse momentum spectra, Eq. (5), including extrapolations to unmeasured regions. A comparison to the alternative method of replacing integrals in the measured regions by sums of data points only brought a negligible contribution to the systematic uncertainty. Extended Data Fig. 7 showed that extrapolations were needed only in the first and last rapidity bin. They amount to 88% and 6.2%, respectively. The large extrapolation in the first bin of rapidity increases the total uncertainty of the corresponding data point shown in Fig. 1 (of the main text). In this figure, the obtained rapidity distribution of the K_S^0 has been fitted with a function consisting of two Gaussians with centers displaced by a value of $\pm\Delta y$ with respect to $y = 0$. These Gaussians have the same widths but may have different amplitudes. The resulting small asymmetry of the fitted rapidity distribution originates from a combined effect of the mass asymmetry of the colliding target and projectile nuclei ($A_{target} = 45$ and $A_{projectile} = 40$) and the selection of central collisions by the energy measured in the kinematic region of the projectile spectator remnants. The former favors backward and the latter forward rapidities. The yields of charged K mesons at mid-rapidity listed in Table 1 (of the main text) were taken from Ref. [18]. They were determined in the interval $0.0 < y < 0.2$ as discussed therein. The yield of neutral K_S^0 mesons at mid-rapidity was determined at $y = 0$ from the aforementioned fit. Its systematic uncertainty was estimated the same way as for the data points (see above), and its statistical uncertainty was obtained by propagation of the statistical uncertainties of the fit. Both statistical and systematic uncertainties of charged and neutral K yields were propagated into the ratio R_K . The additional uncertainty of R_K resulting from the difference in the mid-rapidity definition for charged and neutral mesons was estimated to be 0.5%, about 10% of the total systematic uncertainty.

B. World data

This section presents the yields of charged and neutral kaons measured by various experiments across different collision systems and energies and within specified centrality and rapidity regions. The results, presented in Table 2, are sourced directly from the original experimental publications without any modifications to ensure consistency of the quantities reported. The exceptions are HADES K^+ and K^- yields, where two sources of systematic uncertainties were reported [43]. In our analysis, they were added in quadrature, and the square root of such a sum is shown in Table 2 as the final systematic uncertainty (although in further calculations we used more precise values than 0.0014 and 0.000032 displayed in the table). In the NA49 experiment, the K^+ yield in Pb+Pb at $\sqrt{s_{NN}} = 7.6$ GeV [40] was reported with asymmetric systematic uncertainty; in this case, the upper limit was taken as σ_{sys} . For K^+ and K^- yields in NA35 S+S collisions at $\sqrt{s_{NN}} = 19.4$ GeV only statistical uncertainties were reported in the form of numerical values [38]. We took the NA35 estimate of systematic uncertainty as $\sim 3\%$ [38], and the resulting numerical values are presented in the table. Finally, for the STAR experiment at $\sqrt{s_{NN}} = 130$ GeV [32], two types of uncertainties were reported: uncorrelated errors (first) and correlated systematic errors (second); see Ref. [32] for details.

For all kaon yields reported with statistical and systematic uncertainties separately, we calculated the total uncertainties as $\sigma_{total} = \sqrt{\sigma_{stat}^2 + \sigma_{sys}^2}$ (for STAR at $\sqrt{s_{NN}} = 130$ GeV σ_{total} was taken as $\sqrt{\sigma_{uncorr}^2 + \sigma_{corr}^2}$). Their rounded (to two significant digits) values are displayed in the third column of Table 2 however, more precise values were used when propagating them to σ_{total} of R_K presented in Table 3.

The notation "Yield (4π)" refers to particle mean multiplicity in full phase space. The "Yield ($y \approx 0$)" corresponds to mid-rapidity production, in most cases expressed as rapidity density dn/dy measured in the region specified in Table 2 as "y range" (for CERES results and NA61/SHINE K_S^0 mesons the fits at mid-rapidity were used). In some cases, different intervals were used for charged and neutral kaons. When calculating the charged-to-neutral kaon ratio, we used the originally published results.

The HADES data for Au+Au collisions at $\sqrt{s_{NN}} = 2.4$ GeV [78, 79], the FOPI data for Al+Al collisions at $\sqrt{s_{NN}} = 2.7$ GeV [80, 81], and the NA49 data for Pb+Pb collisions at $\sqrt{s_{NN}} = 17.3$ GeV [41, 42] are excluded from this paper, as the charged and neutral kaons were measured in significantly different centrality intervals. Normalizing these results by the number of participants would introduce model dependence of the R_K ratio. Moreover, we also omit kaon yields evaluated by the Authors of Ref. [82] based on rapidity spectra measured by AGS experiments in Si+Al/Si collisions at $\sqrt{s_{NN}} = 5.4$ GeV. The spectra of charged and neutral kaons were measured for different centralities [82], and the type of presented uncertainties is not clear. Finally, we also exclude NA35 kaon yields from S+Ag collisions at $\sqrt{s_{NN}} = 19.4$ GeV [39, 82]. The type of uncertainties for charged kaon yields [82] is not specified, and the charged and neutral kaons might have been measured for different centralities [39, 82, 83].

NA61/SHINE experiment					
Ar+Sc collisions at $\sqrt{s_{NN}} = 11.9$ GeV					
hadron	Yields ($y \approx 0$) $\pm \sigma_{stat} \pm \sigma_{sys}$	σ_{total}	Centrality	y ranges	Ref.
K^+	$3.732 \pm 0.016 \pm 0.148$	0.15	0–10%	$0.0 < y < 0.2$	[18]
K^-	$2.029 \pm 0.012 \pm 0.069$	0.070	0–10%	$0.0 < y < 0.2$	[18]
K_S^0	$2.433 \pm 0.027 \pm 0.102$	0.11	0–10%	$y = 0$	this analysis
HADES experiment					
Ar+KCl collisions at $\sqrt{s_{NN}} = 2.6$ GeV					
hadron	Yields (4π) $\pm \sigma_{stat} \pm \sigma_{sys}$	σ_{total}	Centrality	y ranges	Ref.
K^+	$0.028 \pm 0.002 \pm 0.0014$ (*)	0.0024	0–35%	extrapolated to 4π	[43]
K^-	$0.00071 \pm 0.00015 \pm 0.000032$ (*)	0.00015	0–35%	extrapolated to 4π	[43]
K_S^0	$0.0115 \pm 0.0005 \pm 0.0009$	0.0010	0–35%	extrapolated to 4π	[44]
STAR (BES I) experiment					
Au+Au collisions at $\sqrt{s_{NN}} = 7.7$ GeV					
hadron	Yields ($y \approx 0$) $\pm \sigma_{stat} \pm \sigma_{sys}$	σ_{total}	Centrality	y ranges	Ref.
K^+	20.8	1.7	0–5%	$-0.1 < y < 0.1$	[30]
K^-	7.7	0.6	0–5%	$-0.1 < y < 0.1$	[30]
K_S^0	$12.67 \pm 0.12 \pm 0.44$	0.46	0–5%	$-0.5 < y < 0.5$	[31]
STAR (BES I) experiment					
Au+Au collisions at $\sqrt{s_{NN}} = 11.5$ GeV					
hadron	Yields ($y \approx 0$) $\pm \sigma_{stat} \pm \sigma_{sys}$	σ_{total}	Centrality	y ranges	Ref.
K^+	25.0	2.5	0–5%	$-0.1 < y < 0.1$	[30]

K^-	12.3	1.2	0–5%	$-0.1 < y < 0.1$	[30]
K_S^0	$15.93 \pm 0.12 \pm 0.58$	0.59	0–5%	$-0.5 < y < 0.5$	[31]
STAR (BES I) experiment					
Au+Au collisions at $\sqrt{s_{NN}} = 19.6$ GeV					
hadron	Yields ($y \approx 0$) $\pm \sigma_{stat} \pm \sigma_{sys}$	σ_{total}	Centrality	y ranges	Ref.
K^+	29.6	2.9	0–5%	$-0.1 < y < 0.1$	[30]
K^-	18.8	1.9	0–5%	$-0.1 < y < 0.1$	[30]
K_S^0	$20.89 \pm 0.08 \pm 0.67$	0.67	0–5%	$-0.5 < y < 0.5$	[31]
STAR (BES I) experiment					
Au+Au collisions at $\sqrt{s_{NN}} = 27$ GeV					
hadron	Yields ($y \approx 0$) $\pm \sigma_{stat} \pm \sigma_{sys}$	σ_{total}	Centrality	y ranges	Ref.
K^+	31.1	2.8	0–5%	$-0.1 < y < 0.1$	[30]
K^-	22.6	2.0	0–5%	$-0.1 < y < 0.1$	[30]
K_S^0	$23.24 \pm 0.09 \pm 0.70$	0.71	0–5%	$-0.5 < y < 0.5$	[31]
STAR (BES I) experiment					
Au+Au collisions at $\sqrt{s_{NN}} = 39$ GeV					
hadron	Yields ($y \approx 0$) $\pm \sigma_{stat} \pm \sigma_{sys}$	σ_{total}	Centrality	y ranges	Ref.
K^+	32.0	2.9	0–5%	$-0.1 < y < 0.1$	[30]
K^-	25.0	2.3	0–5%	$-0.1 < y < 0.1$	[30]
K_S^0	$24.9 \pm 0.1 \pm 1.7$	1.7	0–5%	$-0.5 < y < 0.5$	[31]
NA49 experiment					
Pb+Pb collisions at $\sqrt{s_{NN}} = 7.6$ GeV					
hadron	Yields (4π) $\pm \sigma_{stat} \pm \sigma_{sys}$	σ_{total}	Centrality	y ranges	Ref.
K^+	$52.9 \pm 0.9 \pm 3.5$ (*)	3.6	0–7.2%	extrapolated to 4π	[40]
K^-	$16.0 \pm 0.2 \pm 0.4$	0.45	0–7.2%	extrapolated to 4π	[40]
K_S^0	$29.3 \pm 0.3 \pm 2.9$	2.9	0–7.2%	extrapolated to 4π	[42]
NA49 experiment					
Pb+Pb collisions at $\sqrt{s_{NN}} = 8.7$ GeV					
hadron	Yields (4π) $\pm \sigma_{stat} \pm \sigma_{sys}$	σ_{total}	Centrality	y ranges	Ref.
K^+	$59.1 \pm 1.9 \pm 3$	3.6	0–7.2%	extrapolated to 4π	[41]
K^-	$19.2 \pm 0.5 \pm 1.0$	1.1	0–7.2%	extrapolated to 4π	[41]
K_S^0	$34.2 \pm 0.2 \pm 3.4$	3.4	0–7.2%	extrapolated to 4π	[42]
CERES experiment					
Pb+Au collisions at $\sqrt{s_{NN}} = 17.3$ GeV					
hadron	Yields ($y \approx 0$) $\pm \sigma_{stat} \pm \sigma_{sys}$	σ_{total}	Centrality	y ranges	Ref.
K^+	$31.8 \pm 0.6 \pm 2.5$	2.6	0–7%	$y = 0$	[27]
K^-	$19.3 \pm 0.4 \pm 2.0$	2.0	0–7%	$y = 0$	[27]
K_S^0	$21.2 \pm 0.9 \pm 1.7$	1.9	0–7%	$y = 0$	[28, 29]
NA35 experiment					
S+S collisions at $\sqrt{s_{NN}} = 19.4$ GeV					
hadron	Yields (4π) $\pm \sigma_{stat} \pm \sigma_{sys}$	σ_{total}	Centrality	y ranges	Ref.
K^+	$12.5 \pm 0.4 \pm 0.375$ (*)	0.55	0–2%	extrapolated to 4π	[38]
K^-	$6.9 \pm 0.4 \pm 0.207$ (*)	0.45	0–2%	extrapolated to 4π	[38]
K_S^0	10.5	1.7	0–2%	extrapolated to 4π	[39]

STAR experiment					
Au+Au collisions at $\sqrt{s_{NN}} = 62.4$ GeV					
hadron	Yields ($y \approx 0$) $\pm \sigma_{stat} \pm \sigma_{sys}$	σ_{total}	Centrality	y ranges	Ref.
K^+	37.6	2.7	0–5%	$-0.1 < y < 0.1$	[33]
K^-	32.4	2.3	0–5%	$-0.1 < y < 0.1$	[33]
K_S^0	$27.4 \pm 0.6 \pm 2.9$	3.0	0–5%	$-1 < y < 1$	[34]
STAR experiment					
Au+Au collisions at $\sqrt{s_{NN}} = 130$ GeV					
hadron	Yields ($y \approx 0$) $\pm \sigma_{uncorr} \pm \sigma_{corr}$	σ_{total}	Centrality	y ranges	Ref.
K^+	$46.2 \pm 0.6 \pm 6.0$	6.0	0–6%	$_{-0.5}^{-0.1} < y < \begin{smallmatrix} 0.1 \\ 0.5 \end{smallmatrix}$	[32]
K^-	$41.9 \pm 0.6 \pm 5.4$	5.4	0–6%	$_{-0.5}^{-0.1} < y < \begin{smallmatrix} 0.1 \\ 0.5 \end{smallmatrix}$	[32]
K_S^0	$33.9 \pm 1.1 \pm 5.1$	5.2	0–6%	$-0.5 < y < 0.5$	[32]
STAR experiment					
Au+Au collisions at $\sqrt{s_{NN}} = 200$ GeV					
hadron	Yields ($y \approx 0$) $\pm \sigma_{stat} \pm \sigma_{sys}$	σ_{total}	Centrality	y ranges	Ref.
K^+	51.3	6.5	0–5%	$-0.1 < y < 0.1$	[33]
K^-	49.5	6.2	0–5%	$-0.1 < y < 0.1$	[33]
K_S^0	43.5	2.4	0–5%	$-0.5 < y < 0.5$	[35]
ALICE experiment					
Pb+Pb collisions at $\sqrt{s_{NN}} = 2760$ GeV					
hadron	Yields ($y \approx 0$) $\pm \sigma_{stat} \pm \sigma_{sys}$	σ_{total}	Centrality	y ranges	Ref.
K^+	109	9	0–5%	$-0.5 < y < 0.5$	[36]
K^-	109	9	0–5%	$-0.5 < y < 0.5$	[36]
K_S^0	110	10	0–5%	$-0.5 < y < 0.5$	[37]

Table 2: The compilation of world data on charged and neutral kaon yields in nucleus-nucleus collisions. The yields labeled $y \approx 0$ and 4π correspond to the rapidity density at mid-rapidity and mean multiplicity in full phase space. The uncertainty fields are left empty in case they are not published. The systematic uncertainties labeled by (*) were estimated for this analysis based on the information given in the original papers (see the text). Only results corresponding to the same centrality for charged and neutral kaons are compiled. The "y range" specifies the rapidity range used to obtain a given kaon yield.

Table 3 presents the ratios of charged-to-neutral kaons from various experiments, with estimated statistical and total uncertainties where available. Taking into account the possibility of using our compilation in future analyses, the numerical values in Table 3 are presented with unusually high precision.

Experiment	Collision system	$\sqrt{s_{NN}}$ (GeV)	R_K	σ_{stat}	σ_{total}
NA61/SHINE	Ar+Sc	11.9	1.1839	0.0138	0.0615
HADES	Ar+KCl	2.6	1.2483	0.1027	0.1545
STAR (BES I)	Au+Au	7.7	1.1247	-	0.0819
STAR (BES I)	Au+Au	11.5	1.1707	-	0.0973
STAR (BES I)	Au+Au	19.6	1.1584	-	0.0910
STAR (BES I)	Au+Au	27	1.1553	-	0.0819
STAR (BES I)	Au+Au	39	1.1446	-	0.1079

NA49	Pb+Pb	7.6	1.1758	0.0198	0.1325
NA49	Pb+Pb	8.7	1.1447	0.0295	0.1263
CERES	Pb+Au	17.3	1.2052	0.0539	0.1340
NA35	S+S	19.4	0.9238	-	0.1533
STAR	Au+Au	62.4	1.2774	-	0.1525
STAR	Au+Au	130	1.2994	-	0.2331
STAR	Au+Au	200	1.1586	-	0.1214
ALICE	Pb+Pb	2760	0.9909	-	0.1071

Table 3: Ratios of charged kaons to neutral kaons in different experiments.

C. Models

Hadron Resonance Gas Model. We use the Hadron Resonance Gas model implementation from Ref. [15] to quantify the isospin-breaking effects and their interplay. HRG includes all hadrons and resonances with confirmed status in the PDG tables [84]. The PDG-listed masses, charges, lifetimes, and decay modes are used. Thus, HRG includes the isospin-symmetry violation due to masses and branching ratios of hadrons and resonances.

In HRG calculations, the exact net strangeness conservation is enforced, i.e., the calculations are done within the strangeness canonical ensemble (SCE) [85, 86]. The model parameters are baryo-chemical potential, μ_B , temperature, T , volume of the system V , and the strangeness under-saturation parameter γ_S (see Ref. [87]). We adopt the simple parametrization of μ_B and T as a function of collision energy introduced in Ref. [88]. We have checked that R_K is weakly sensitive to the strangeness suppression effect introduced by having the parameter $\gamma_S < 1$. Therefore, calculations are done for $\gamma_S = 1$ for simplicity. The energy-dependent Breit-Wigner spectra [89] model the resonance widths.

Figure 3 (black line) shows the HRG predictions for R_K as a function of collision energy $\sqrt{s_{NN}}$ for $Q/B = 0.4$. At low collision energies, $R_K < 1$ due to the enhancement of neutral kaon production caused by a larger number of neutrons than protons, $Q/B < 1/2$. On the other hand, at high collision energies, HRG predicts $R_K \approx 1.018$ due to the mass difference between charged and neutral kaons produced directly. Finally, $R_K \approx 1.032$ when kaon production via resonance decays is included. This is mostly due to ϕ decays, which strongly prefer the decay into charged kaons over the one into neutral kaons.

We have checked that the system electric to baryon charge ratio Q/B significantly affects R_K up to $\sqrt{s_{NN}} \approx 10$ GeV. At higher energies, pions dominate, and total electric and baryon charges are significantly larger than the corresponding net charges. Thus, R_K becomes increasingly less sensitive to Q/B with an increase in $\sqrt{s_{NN}}$.

We have checked that the strangeness grand-canonical ensemble and other popular parametrizations [47, 90] of the model parameters as a function of collision energy lead to quantitatively similar results for R_K , for $\sqrt{s_{NN}} \gtrsim 4$ GeV. The uncertainties of R_K estimated by changing the parametrization of model parameters [88] are less than 1% for $\sqrt{s_{NN}} > 3$ GeV. The effect of including light nuclei in the particle list is negligible.

UrQMD model. The UrQMD transport model [16, 45, 46] describes A+A collisions by explicitly propagating hadrons in phase space. During the propagation, rescattering among hadrons takes place. The particle

production in this model happens via resonance decay or string excitation and fragmentation following the LUND model [91].

The gray squares in Fig. 3 indicate the UrQMD model predictions. Here, we have considered central Au+Au collisions ($A = 197$, $Z = 79$, $Q/B \approx 0.4$). The predictions are shown within the $\sqrt{s_{NN}}$ range of 2.4 to 20 GeV. At each energy, 10^4 events are used for the analysis.

One sees that for $\sqrt{s_{NN}} \lesssim 7$ GeV, the predictions of UrQMD and HRG are similar. At higher energies, the R_K ratio in HRG is systematically higher than the one predicted by UrQMD. This is likely caused by UrQMD assuming ϕ -meson decays to be exactly isospin symmetric instead of taking the branching ratios from PDG. This is the reason for showing the UrQMD predictions only up to 20 GeV.

Extended Data

rapidity bin		(-1.5, -1)	(-1, -0.5)	(-0.5, 0)	(0, 0.5)	(0.5, 1)	(1, 1.5)	(1.5, 2)
cut value	cosine of angle	>0.999	>0.9995	>0.9995	>0.9995	>0.9995	>0.9999	>0.9999
	distance	>5 cm	>5 cm	>7.5 cm	>12.5 cm	>12.5 cm	>15 cm	>12.5 cm

Table 4: Track pair cuts. Values of the cuts on (top row) the cosine of the angle between the line joining the primary and decay vertex and the direction of the vector sum of decay daughter momenta, and (bottom row) the distance between the primary and decay vertex.

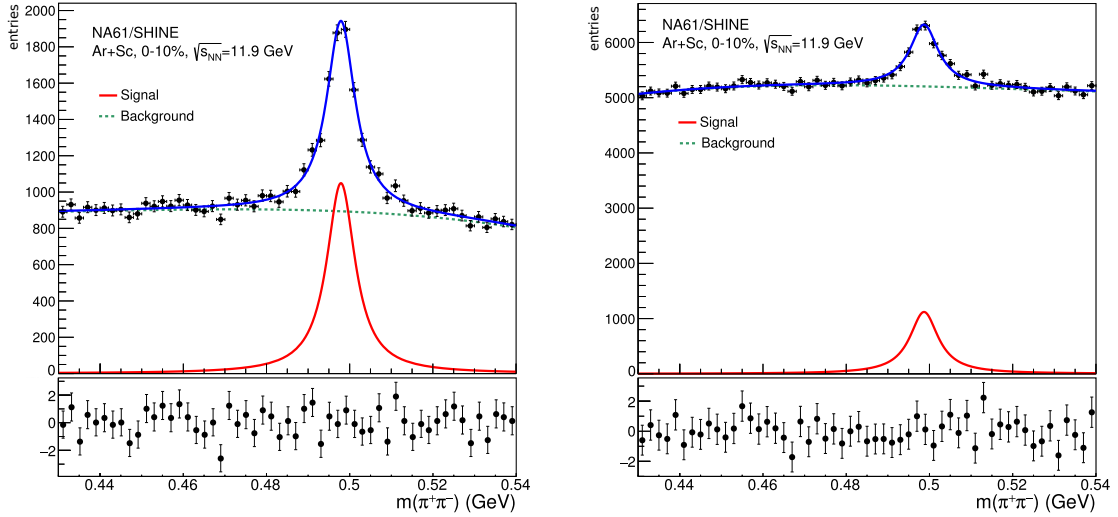


Figure 5: Examples of fitted invariant mass distributions. Two studied bins in rapidity y and transverse momentum p_T of the K_S^0 are presented, left: $y \in (-1.0, -0.5)$, $p_T \in (1.2, 1.5)$ GeV/ c , right: $y \in (0.5, 1.0)$, $p_T \in (1.2, 1.5)$ GeV/ c . The bottom panels show the difference between the experimental data and the fitted (Signal+Background) distribution, divided by the experimental uncertainty.

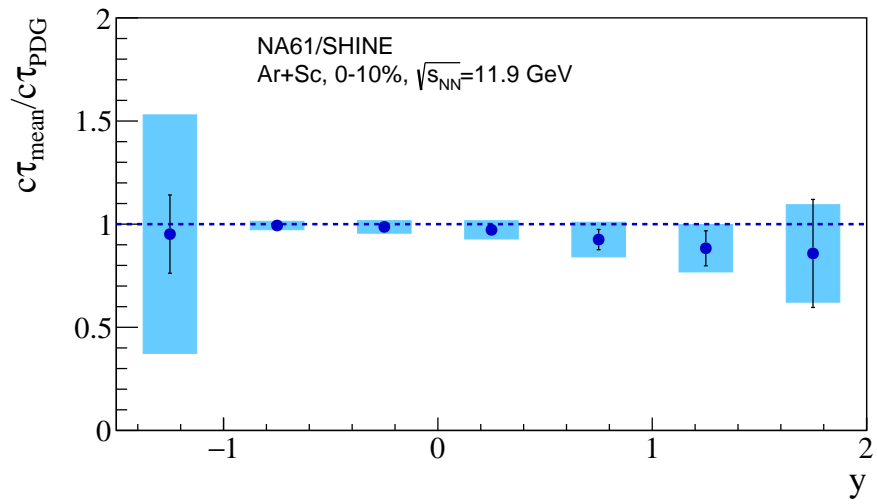


Figure 6: Mean lifetime of K_S^0 mesons as a function of rapidity. The values obtained by NA61/SHINE are divided by the PDG value [3]. Statistical uncertainties are shown by vertical bars and systematic ones by shaded boxes.

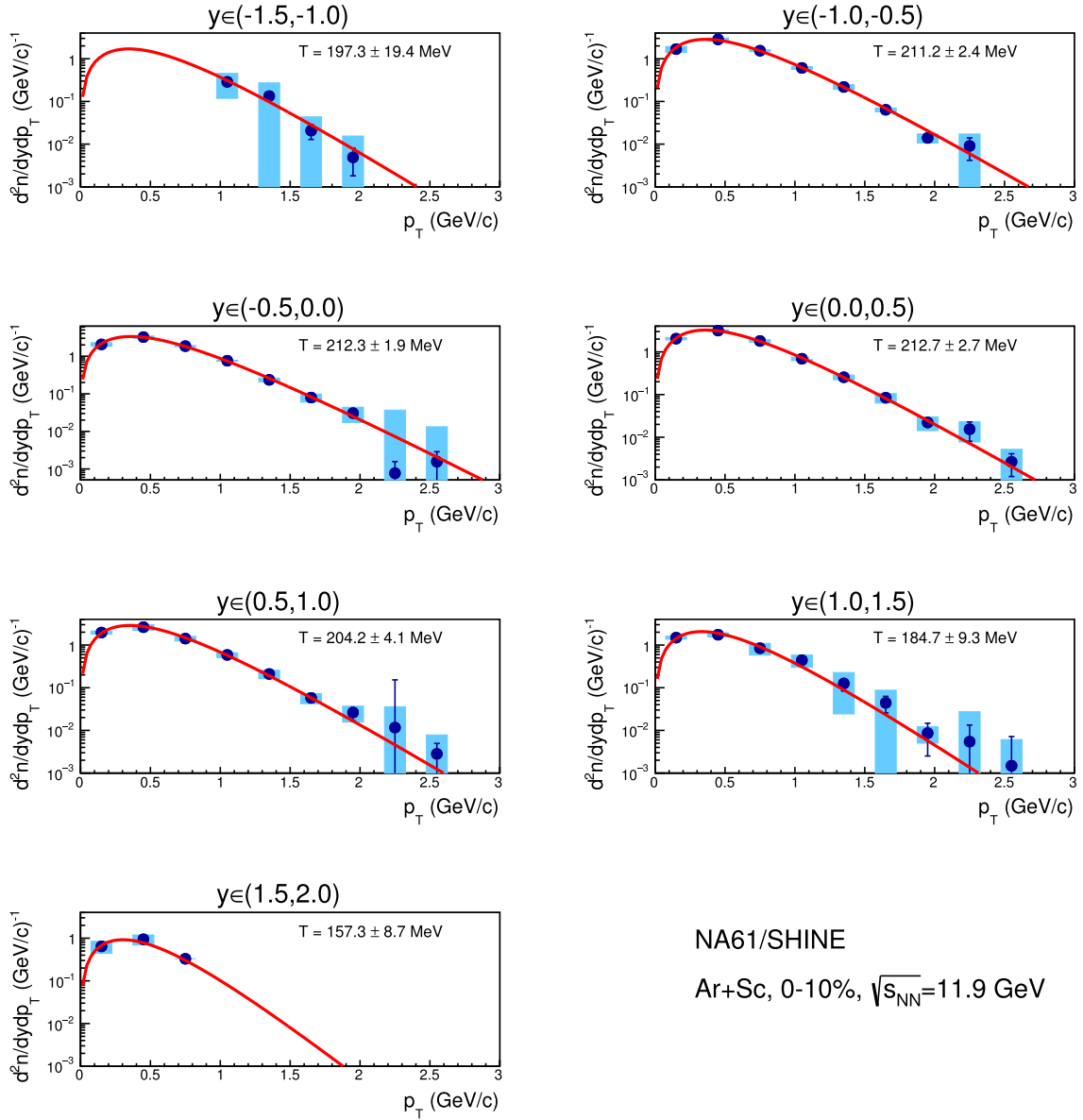






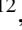





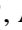

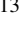




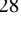



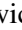
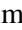


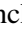




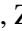


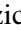





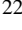



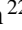
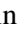
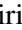












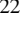


































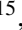





















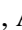





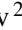











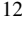
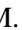

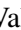


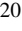






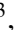



Figure 7: K_S^0 transverse momentum spectra in rapidity bins. Statistical uncertainties are shown by vertical bars and systematic ones by shaded boxes. Red curves represent fits of the data with the function defined in Eq. (5). The inverse slope parameters (T), with their statistical uncertainties resulting from the fits, are also displayed inside the panels.

The NA61/SHINE Collaboration

H. Adhikary ¹³, P. Adrich ¹⁵, K.K. Allison ²⁶, N. Amin ⁵, E.V. Andronov ²², I.-C. Arsene ¹², M. Bajda ¹⁶, Y. Balkova ¹⁸, D. Battaglia ²⁵, A. Bazgir ¹³, S. Bhosale ¹⁴, M. Bielewicz ¹⁵, A. Blondel ⁴, M. Bogomilov ², Y. Bondar ¹³, A. Brandin ²², W. Bryliński ²¹, J. Brzychczyk ¹⁶, M. Buryakov ²², A.F. Camino ²⁸, M. Čirković ²³, M. Csanád ⁸, J. Cybowska ²¹, T. Czopowicz ¹³, C. Dalmazzone ⁴, N. Davis ¹⁴, A. Dmitriev ²², P. von Doetinchem ²⁷, W. Dominik ¹⁹, J. Dumarchez ⁴, R. Engel ⁵, G.A. Feofilov ²², L. Fields ²⁵, Z. Fodor ^{7,20}, M. Friend ⁹, M. Gaździcki ¹³, O. Golosov ²², V. Golovatyuk ²², M. Golubeva ²², K. Grebieszko ²¹, F. Guber ²², S.N. Igolkin ²², S. Ilieva ², A. Ivashkin ²², A. Izvestnyy ²², N. Kargin ²², N. Karpushkin ²², E. Kashirin ²², M. Kiełbowicz ¹⁴, V.A. Kireyeu ²², R. Kolesnikov ²², D. Kolev ², Y. Koshio ¹⁰, V.N. Kovalenko ²², S. Kowalski ¹⁸, B. Kozłowski ²¹, A. Krasnoperov ²², W. Kucewicz ¹⁷, M. Kuchowicz ²⁰, M. Kuich ¹⁹, A. Kurepin ²², A. László ⁷, M. Lewicki ²⁰, G. Lykasov ²², V.V. Lyubushkin ²², M. Maćkowiak-Pawłowska ²¹, Z. Majka ^{16†}, A. Makhnev ²², B. Maksiak ¹⁵, A.I. Malakhov ²², A. Marcinek ¹⁴, A.D. Marino ²⁶, H.-J. Mathes ⁵, T. Matulewicz ¹⁹, V. Matveev ²², G.L. Melkumov ²², A. Merzlaya ¹², Ł. Mik ¹⁷, S. Morozov ²², Y. Nagai ⁸, T. Nakadaira ⁹, M. Naskret ²⁰, S. Nishimori ⁹, A. Olivier ²⁵, V. Ozvenchuk ¹⁴, O. Panova ¹³, V. Paolone ²⁸, O. Petukhov ²², I. Pidhurskyi ¹³, R. Płaneta ¹⁶, P. Podlaski ¹⁹, B.A. Popov ^{22,4}, B. Pórfy ^{7,8}, D.S. Prokhorova ²², D. Pszczel ¹⁵, S. Puławski ¹⁸, J. Puzović ^{23†}, R. Renfordt ¹⁸, L. Ren ²⁶, V.Z. Reyna Ortiz ¹³, D. Röhrich ¹¹, E. Rondio ¹⁵, M. Roth ⁵, Ł. Rozpłochowski ¹⁴, B.T. Rumberger ²⁶, M. Romyantsev ²², A. Rustamov ¹, M. Rybczynski ¹³, A. Rybicki ¹⁴, D. Rybka ¹⁵, K. Sakashita ⁹, K. Schmidt ¹⁸, A.Yu. Seryakov ²², P. Seyboth ¹³, U.A. Shah ¹³, Y. Shiraishi ¹⁰, A. Shukla ²⁷, M. Słodkowski ²¹, P. Staszal ¹⁶, G. Stefanek ¹³, J. Stepaniak ¹⁵, M. Strikhanov ²², H. Ströbele ⁶, T. Šušar ³, Ł. Świdorski ¹⁵, J. Szewiński ¹⁵, R. Szukiewicz ²⁰, A. Taranenko ²², A. Tefelska ²¹, D. Tefelski ²¹, V. Tereshchenko ²², R. Tsenov ², L. Turko ²⁰, T.S. Tveter ¹², M. Unger ⁵, M. Urbaniak ¹⁸, F.F. Valiev ²², D. Veberič ⁵, V.V. Vechernin ²², O. Vitiuk ²⁰, V. Volkov ²², A. Wickremasinghe ²⁴, K. Witek ¹⁷, K. Wójcik ¹⁸, O. Wyszynski ¹³, A. Zaitsev ²², E. Zherebtsova ²⁰, E.D. Zimmerman ²⁶, A. Zviagina ²², and R. Zwaska ²⁴

and the Theory Group

F. Giacosa ^{13,6} M. Gorenstein ^{29,30} R. Poberezhniuk ^{29,30,31} S. Samanta ³²

[†] deceased

¹ National Nuclear Research Center, Baku, Azerbaijan

² Faculty of Physics, University of Sofia, Sofia, Bulgaria

³ Ruder Bošković Institute, Zagreb, Croatia

⁴ LPNHE, Sorbonne University, CNRS/IN2P3, Paris, France

⁵ Karlsruhe Institute of Technology, Karlsruhe, Germany

⁶ University of Frankfurt, Frankfurt, Germany

- ⁷ HUN-REN Wigner Research Centre for Physics, Budapest, Hungary
- ⁸ Eötvös Loránd University, Budapest, Hungary
- ⁹ Institute for Particle and Nuclear Studies, Tsukuba, Japan
- ¹⁰ Okayama University, Japan
- ¹¹ University of Bergen, Bergen, Norway
- ¹² University of Oslo, Oslo, Norway
- ¹³ Jan Kochanowski University, Kielce, Poland
- ¹⁴ Institute of Nuclear Physics, Polish Academy of Sciences, Cracow, Poland
- ¹⁵ National Centre for Nuclear Research, Warsaw, Poland
- ¹⁶ Jagiellonian University, Cracow, Poland
- ¹⁷ AGH - University of Science and Technology, Cracow, Poland
- ¹⁸ University of Silesia, Katowice, Poland
- ¹⁹ University of Warsaw, Warsaw, Poland
- ²⁰ University of Wrocław, Wrocław, Poland
- ²¹ Warsaw University of Technology, Warsaw, Poland
- ²² Affiliated with an institution covered by a cooperation agreement with CERN
- ²³ University of Belgrade, Belgrade, Serbia
- ²⁴ Fermilab, Batavia, USA
- ²⁵ University of Notre Dame, Notre Dame, USA
- ²⁶ University of Colorado, Boulder, USA
- ²⁷ University of Hawaii at Manoa, Honolulu, USA
- ²⁸ University of Pittsburgh, Pittsburgh, USA
- ²⁹ Bogolyubov Institute for Theoretical Physics, Kyiv, Ukraine
- ³⁰ Frankfurt Institute for Advanced Studies, Giersch Science Center, Frankfurt am Main, Germany
- ³¹ University of Houston, Houston, USA
- ³² School of Applied Sciences, Kalinga Institute of Industrial Technology, Bhubaneswar, Odisha, India